

A UNIFIED FORMULATION FOR GEOMETRIC CONSERVATION BASED MULTIFLUID ALGORITHMS

M. DARWISH
American University of Beirut,
Faculty of Engineering & Architecture,
Mechanical Engineering Department,
P.O.Box 11-0236
Beirut – Lebanon
Email: darwish@aub.edu.lb

F. MOUKALLED
American University of Beirut,
Faculty of Engineering & Architecture,
Mechanical Engineering Department,
P.O.Box 11-0236
Beirut – Lebanon
Email: memouk@aub.edu.lb

Keywords: Finite-volume methods, Multi-fluid algorithms, Pressure-Based algorithms, Bubbly Flow, Air-Particle Flow

ABSTRACT

Over the past two decades important advances have taken place in CFD centered around increasing numerical accuracy through the development of high-resolution schemes and improving efficiency through devising better solution algorithms, better solvers, and increasing use of multigrid techniques. For the solution of single-fluid flow, a number of segregated solution algorithms have been developed such as the well-known SIMPLE [1], the PISO[2], and the SIMPLEX [3] algorithms, to cite a few. Additionally, several techniques to improve the performance, facilitate the implementation, and extend the capability of these algorithms have been advertised [4]. On the other hand, developments in segregated multi-fluid solution algorithms have not been as fortunate due to both the higher computational cost involved and the numerical difficulties that had to be first addressed in the simulation of single-fluid flow. Despite these difficulties, the SIMPLE approach has been extended to multi-fluid flow simulations through the development of the Inter-Phase Slip Algorithm (IPSA) and its variants by the Spalding Group at Imperial College [5,6,7] and the Implicit Multi-Field [8] algorithms (IMF) by the Los Alamos Scientific Laboratory (LASL) group [9,10,11,12,13]. However, in contrast with the widespread information available on single-fluid solution algorithms, much less

information is available on multi-fluid solution algorithms, a fact that has confined their implementation to a small community, slowed their development, and isolated them from the newer developments in single-fluid flow algorithms.

Darwish et.al. [14] showed that all segregated single-fluid pressure-based algorithms can be extended to multi-fluid flow simulations. This extension can be accomplished in two different ways depending on the constraint equation used in deriving the pressure correction equation. The Mass Conservation Based Algorithms (MCBA) and the Geometric Conservation Based Algorithms (GCBA) denoted the resulting two families. Having introduced the MCBA in a previous article [**Error! Bookmark not defined.**], this paper presents the GCBA family, in which, the pressure correction equation is derived using, as a constraint, the overall volume conservation equation. The new GCBA based algorithm that accounts implicitly for the volume fraction-pressure-velocity coupling is also introduced. The formulation is done using a unified, compact, and easy to understand notation that can be expanded systematically to yield the coefficients of the pressure correction equation. Results for compressible and incompressible test problems are also presented.

INTRODUCTION

Multifluid flow algorithms are inherently more complex than their single fluid counterpart. This is partly due to the increase in the number of momentum and continuity equations that need to be solved and thus in resolving the velocity-pressure coupling and to the additional inter-fluid coupling that is due to fluid-fluid interaction. One important aspect of multifluid flow algorithms is in how the geometric conservation law (mathematically expressed as sum of volume fraction equal 1) is resolved. In Mass Conservation Based Algorithm (MCBA) the geometric conservation law is decoupled from the velocity-pressure algorithm, the pressure correction equation is thus derived using a mass conservation constraint [14] (Global mass conservation) and used for the correction of the velocity and pressure fields in addition to the density for compressible flows. In Geometric Conservation Based Algorithms (GCBA), the pressure equation is derived from the geometric conservation law expressed mathematically as sum of fluidic volume fractions equal 1. This approach enables the coupling of the volume fraction to the velocity, pressure (and density) fields, the derived pressure correction equation is thus used for the correction of the pressure, velocity and volume fraction fields, in addition to the density field for compressible flows. In this paper the GCBA formulation is presented using a unified notation and seven GCBA-based segregated algorithms (SIMPLE, PISO, SIMPLEX, SIMPLEC, SIMPLEM, SIMPLEST, and PRIME) are used in solving two test problems involving incompressible and compressible fluids, namely simulation of turbulent upward bubbly flow in a pipe and simulation of dilute air-particle flow over a flat plate. For both problems the convergence histories of the GCBA-based algorithms are quite similar (except for PRIME). This underlines, in the authors' view, the importance of resolving volume fractions coupling implicitly in multifluid flow algorithms

NOMENCLATURE

$A_p^{(k)}$... coefficients in the discretized equation for $\phi^{(k)}$.
 $B_p^{(k)}$ source term in the discretized equation for $\phi^{(k)}$.
 $\mathbf{B}^{(k)}$ body force per unit volume of fluid/phase k.
 $C_\rho^{(k)}$ coefficient equals to $1/R^{(k)}T^{(k)}$.
 $D_p^{(k)}[\phi^{(k)}]$ the D operator.
 $\mathbf{D}_p^{(k)}[\phi^{(k)}]$ the vector form of the D operator.
 $H_p[\phi^{(k)}]$ the H operator.
 $\mathbf{HP}_p[\mathbf{u}^{(k)}]$ the vector form of the HP operator.
 $\tilde{\mathbf{HP}}_p[\mathbf{u}^{(k)}]$ the vector form of the modified HP operator.
 $\mathbf{I}^{(k)}$ inter-phase momentum transfer.
 $\mathbf{J}_f^{(k)D}$ diffusion flux of $\phi^{(k)}$ across cell face 'f'.
 $\mathbf{J}_f^{(k)C}$ convection flux of $\phi^{(k)}$ across cell face 'f'.

$M^{(k)}$ mass source per unit volume.
 P pressure.
 $Q^{(k)}$ general source term of fluid/phase k.
 $r^{(k)}$ volume fraction of fluid/phase k.
 $R^{(k)}$ gas constant for fluid/phase k.
 \mathbf{S}_f surface vector.
 $T^{(k)}$ temperature of fluid/phase k.
 $\mathbf{u}^{(k)}$ velocity vector of fluid/phase k.
 $u^{(k)}, v^{(k)}, \dots$ velocity components of fluid/phase k.

Greek Symbols

$\rho^{(k)}$ density of fluid/phase k.
 $\Gamma^{(k)}$ diffusion coefficient of fluid/phase k.
 $\Phi^{(k)}$ dissipation term in energy equation of fluid/phase k.
 $\phi^{(k)}$ general scalar quantity associated with fluid/phase k.
 $\Delta_p[\phi^{(k)}]$ the Δ operator.
 $\mu^{(k)}$ viscosity of fluid/phase k.
 Ω cell volume.
 δt time step.
 γ scaling factor.

Subscripts

e, w, ... refers to the faces of a control volume.
E, W, ... refers to the neighbors of the main grid point.
f refers to control volume face f.
P refers to the P grid point.

Superscripts

C refers to convection contribution.
D refers to diffusion contribution.
(k) refers to fluid/phase k.

THE GOVERNING EQUATIONS

The equations governing multi-fluid flows are the conservation laws of mass, momentum, and energy for each individual fluid in addition to a set of auxiliary relations.

Conservation of mass

The volume fraction $r^{(k)}$, which is the proportion of volumetric space occupied by the k^{th} fluid ($\Omega^{(k)}/\Omega$) along with the k^{th} fluid density, $\rho^{(k)}$, and velocity, $\mathbf{u}^{(k)}$, in order to satisfy the mass-conservation principle, have to obey the differential equation:

$$\frac{\partial(r^{(k)}\rho^{(k)})}{\partial t} + \nabla \cdot (r^{(k)}\rho^{(k)}\mathbf{u}^{(k)}) = r^{(k)}M^{(k)} \quad (1)$$

Mass sources are often non-zero, as when one fluid is transformed to another fluid. However, summation over all fluids leads to the following "overall mass-conservation" equation:

$$\sum_k \left(\frac{\partial(r^{(k)}\rho^{(k)})}{\partial t} + \nabla \cdot (r^{(k)}\rho^{(k)}\mathbf{u}^{(k)}) \right) = 0 \quad (2)$$

The zero on the right-hand side signifies that the sum of mass sources (generation and loss) is zero.

Conservation of momentum

Denoting the velocity of the k^{th} phase by $\mathbf{u}^{(k)}$, then the momentum equation for the k^{th} phase can be written as:

$$\begin{aligned} & \frac{\partial(r^{(k)} \rho^{(k)} \mathbf{u}^{(k)})}{\partial t} + \nabla \cdot (r^{(k)} \rho^{(k)} \mathbf{u}^{(k)} \mathbf{u}^{(k)}) \\ &= \nabla \cdot (r^{(k)} \mu^{(k)} \nabla \mathbf{u}^{(k)}) + r^{(k)} (-\nabla P + \mathbf{B}^{(k)}) + \mathbf{I}^{(k)} \end{aligned} \quad (3)$$

Here P stands for the pressure, which is regarded as being shared by the fluids, $\mathbf{B}^{(k)}$ is the body force per unit volume of phase (k) , $\mathbf{I}^{(k)}$ is the momentum transfer to phase (k) resulting from interaction with other phases and can be written in the following form

$$\mathbf{I}^{(k)} = \sum_{m=(\text{phases} \neq k)} g^{(km)} (\mathbf{u}^{(m)} - \mathbf{u}^{(k)}) \quad (4)$$

Conservation of energy

Let $T^{(k)}$ be the temperature of the k^{th} phase, then the energy equation for the k^{th} phase is given by:

$$\begin{aligned} & \frac{\partial(r^{(k)} \rho^{(k)} T^{(k)})}{\partial t} + \nabla \cdot (r^{(k)} \rho^{(k)} \mathbf{u}^{(k)} T^{(k)}) \\ &= \frac{1}{c_p^{(k)}} \nabla \cdot (r^{(k)} k^{(k)} \nabla T^{(k)}) + \frac{r^{(k)}}{c_p^{(k)}} \{\Phi^{(k)} + \Phi^{(k)}\} \\ &+ \frac{r^{(k)}}{c_p^{(k)}} \left\{ \beta^{(k)} T^{(k)} \left[\frac{\partial P}{\partial t} + \nabla \cdot (P \mathbf{u}^{(k)}) - P \nabla \cdot (\mathbf{u}^{(k)}) \right] \right\} \end{aligned} \quad (5)$$

where $\Phi^{(k)}$ is the viscous dissipation function of the k^{th} phase and $\beta^{(k)}$ the thermal expansion coefficient of the k^{th} phase which is equal to $1/T^{(k)}$ for an ideal gas.

General Multi-Fluid Scalar Equation

A review of the above differential equations reveals that they are similar in structure. If a typical representative variable associated with phase (k) is denoted by $\phi^{(k)}$, the general differential equation may be written as:

$$\begin{aligned} & \frac{\partial(r^{(k)} \rho^{(k)} \phi^{(k)})}{\partial t} + \nabla \cdot (r^{(k)} \rho^{(k)} \mathbf{u}^{(k)} \phi^{(k)}) \\ &= \nabla \cdot (r^{(k)} \Gamma^{(k)} \nabla \phi^{(k)}) + r^{(k)} Q^{(k)} \end{aligned} \quad (6)$$

Auxiliary Relations

A number of auxiliary relations (equations of state and geometric conservation) are needed in addition to the boundary and initial conditions to close the equation.

Physically, the geometric conservation equation is a statement indicating that the sum of volumes occupied by the different fluids within a cell is equal to the volume of the cell containing the fluids. Mathematically, it is given by

$$\sum_k r^{(k)} = 1 \quad (7)$$

An auxiliary equation of state relating density to pressure and temperature is needed for each fluid. For the k^{th} fluid, such an equation is written as:

$$\rho^{(k)} = \rho^{(k)}(P, T^{(k)}) \quad (8)$$

In order to represent a complete mathematical problem, thermodynamic relations might be needed, and initial and boundary conditions should supplement the above equations.

DISCRETIZATION PROCEDURE

The discretization follows the standard Finite Volume Method practices. The conservation equations are integrated over a finite volume (Fig. 1) to yield the following expression:

$$\begin{aligned} & \iint_{\Omega} \frac{\partial(r^{(k)} \rho^{(k)} \phi^{(k)})}{\partial t} d\Omega + \iint_{\Omega} \nabla \cdot (r^{(k)} \rho^{(k)} \mathbf{u}^{(k)} \phi^{(k)}) d\Omega \\ &= \iint_{\Omega} \nabla \cdot (r^{(k)} \Gamma^{(k)} \nabla \phi^{(k)}) d\Omega + \iint_{\Omega} r^{(k)} Q^{(k)} d\Omega \end{aligned} \quad (9)$$

where Ω is the volume of the control cell. Using the divergence theorem to transform the volume integral into a surface integral and then replacing the surface integral by a summation of the fluxes over the sides of the control volume, equation (9) is transformed to:

$$\begin{aligned} & \frac{\partial(r^{(k)} \rho^{(k)} \phi^{(k)} \Omega)}{\partial t} + \\ & \sum_{nb=e,w,n,s,t,b} (\mathbf{J}_{nb}^{(k)D} + \mathbf{J}_{nb}^{(k)C}) = r^{(k)} Q^{(k)} \Omega \end{aligned} \quad (10)$$

where $\mathbf{J}_{nb}^{(k)D}$ and $\mathbf{J}_{nb}^{(k)C}$ are the diffusive and convective fluxes, respectively. Substituting the fluxes by their equivalent expressions yields:

$$A_P^{(k)} \phi_P^{(k)} = \sum_{NB} A_{NB}^{(k)} \phi_{NB}^{(k)} + B_P^{(k)} \quad (11)$$

In compact form, the above equation can be written as

$$\phi^{(k)} = H_P [\phi^{(k)}] = \frac{\sum_{NB} A_{NB}^{(k)} \phi_{NB}^{(k)} + B_P^{(k)}}{A_P^{(k)}} \quad (12)$$

For the momentum equation we have:

$$\mathbf{u}_P^{(k)} = \mathbf{H} \mathbf{P}_P [\mathbf{u}^{(k)}] - r^{(k)} \mathbf{D}_P^{(k)} \nabla_P(P) \quad (13)$$

where the body force and inter-phase terms are absorbed in the $\mathbf{B}_P^{(k)}$ source term within the $\mathbf{H} \mathbf{P}_P [\mathbf{u}^{(k)}]$ term.

The fluidic mass-conservation equation can be viewed as a volume fraction equation for the k^{th} fluid in which case it can be discretized and written in the form

$$r_P^{(k)} = H_P [r^{(k)}] \quad (14)$$

or as a continuity equation for the k^{th} fluid, in which case it is written as:

$$\frac{(r_P^{(k)} \rho_P^{(k)}) - (r_P^{(k)} \rho_P^{(k)})^{Old}}{\delta t} \Omega - \quad (15)$$

$$\Delta_P [r^{(k)} \rho_P^{(k)} \mathbf{u}^{(k)} \cdot \mathbf{S}] = r^{(k)} \mathcal{M}^{(k)}$$

where the Δ operator represents the following operation:

$$\Delta_P[\Theta] = \sum_{f=NB(P)} \Theta_f \quad (16)$$

The discretization of the energy equation follows that of the general multi-fluid scalar equation. The only difference is the one pertaining to the discretization of the additional source terms. Since a control volume approach is followed, the integral of these sources over the control volume appears in the discretized equation. By using the divergence theorem, the volume integral is transformed into a surface integral and the resultant discretized expressions are evaluated explicitly.

GEOMETRIC CONSERVATION BASED ALGORITHMS

The sequence of events in the Geometric Conservation Based Algorithm (GCBA) is as follows:

- Solve the individual fluidic mass conservation equations for volume fractions.
- Solve the momentum equations for velocities.
- Solve the pressure correction equation.
- Correct velocity, volume fraction, density, and pressure fields.
- Solve the individual energy equations.
- Return to the first step and repeat until convergence.

The Pressure Correction Equation

After solving the continuity equations for the volume fraction fields and the momentum equations for the velocity fields, the next step is to correct the various fields such that the volume fraction fields satisfy the compatibility equation and the velocity and pressure fields satisfy the continuity equations. In the GCBA, the pressure correction equation is derived from the geometric conservation equation. Noting that initially the volume fraction field denoted by $r^{(k)*}$, does not satisfy the compatibility equation and a discrepancy exists i.e.

$$RESG_P = 1 - \sum_k r_P^{(k)*} \quad (17)$$

A change to $r^{(k)*}$ is sought that would restore the balance. The corrected r value, denoted by $r^{(k)}$ ($r^{(k)} = r^{(k)*} + r^{(k)'}$), is such that

$$\sum_k (r^{(k)'}) = 1 - \sum_k (r^{(k)*}) = RESG_P \quad (18)$$

Correction to the volume fraction, $r^{(k)'}$, will be associated with a correction to the velocity, density, and pressure fields, $\mathbf{u}^{(k)'}$, $\rho^{(k)'}$, and P' respectively. Thus, the corrected fields are given as:

$$\begin{cases} r^{(k)} = r^{(k)*} + r^{(k)'} , P = P^0 + P' \\ \mathbf{u}^{(k)} = \mathbf{u}^{(k)*} + \mathbf{u}^{(k)'}, \rho^{(k)} = \rho^{(k)0} + \rho^{(k)'} \end{cases} \quad (19)$$

Then, neglecting second and third order terms, the discretized form of the corrected continuity equation of phase (k) is given by

$$\begin{aligned} & \left(\frac{r_P^{(k)*} \rho_P^{(k)'} + r_P^{(k)'} \rho_P^{(k)0}}{\delta t} \right) \Omega_P - M_P^{(k)} r_P^{(k)'} \Omega_P + \\ & \Delta_P \left[\left(r^{(k)*} \rho^{(k)0} \mathbf{u}^{(k)'} \cdot \mathbf{S} + r^{(k)*} U^{(k)*} \rho_P^{(k)'} \right) \right. \\ & \left. + \rho^{(k)0} U^{(k)*} r^{(k)'} \right] \quad (20) \\ & = - \left(\frac{r_P^{(k)*} \rho_P^{(k)0} - (r_P^{(k)} \rho_P^{(k)})^{Old}}{\delta t} \right) \Omega_P - \\ & \Delta_P \left[\left(r^{(k)*} \rho^{(k)0} U^{(k)*} \right) \right] + M_P^{(k)} r_P^{(k)*} \Omega_P \end{aligned}$$

Writing $\mathbf{u}^{(k)'}$ as a function of P' , similar to what is usually done in a SIMPLE-like algorithm, the momentum correction equations become

$$\begin{aligned} \mathbf{u}^{(k)'} &= \mathbf{HP}[\mathbf{u}^{(k)'}] - r^{(k)*} \mathbf{D}^{(k)} \nabla P' - \\ r^{(k)'} \mathbf{D}^{(k)} \nabla P^0 &- r^{(k)'} \mathbf{D}^{(k)} \nabla P' \end{aligned} \quad (21)$$

Substituting Eq. (19) into Eq. (18), rearranging, and neglecting the correction to neighboring cells, one obtains, the following equation is obtained:

$$\begin{aligned} r_P^{(k)'} &= \\ & \left(\frac{r_P^{(k)*} \Omega_P}{\delta t} \rho_P^{(k)'} + \right. \\ & \left. \Delta_P \left[r^{(k)*} \rho^{(k)0} \left(\mathbf{HP}[\mathbf{u}^{(k)'}] - r^{(k)*} \mathbf{D}^{(k)} \nabla P' \right) \cdot \mathbf{S} \right. \right. \\ & \left. \left. + r^{(k)'} U^{(k)*} \rho^{(k)'} \right] \right. \\ & \left. + \frac{(r_P^{(k)*} \rho_P^{(k)0}) - (r_P^{(k)} \rho_P^{(k)})^{Old}}{\delta t} \Omega_P \right. \\ & \left. + \Delta_P \left[\left(r^{(k)*} \rho^{(k)0} U^{(k)*} \right) \right] - M_P^{(k)} r_P^{(k)*} \Omega_P \right) \end{aligned} \quad (22)$$

where $R_P^{(k)} = 1/A_P^{(k)}$

Substituting this equation into the geometric conservation equation and replacing density correction by pressure correction (i.e. $\rho^{(k)'} = C_\rho^{(k)} P'$), equation (34) is transformed to

$$\begin{aligned} & \left(\frac{r_P^{(k)*} \Omega_P C_\rho^{(k)}}{\delta t} P' + \right. \\ & \left. \Delta_P \left[r^{(k)*} U^{(k)*} C_\rho^{(k)} P' \right] + \right. \\ & \left. \Delta_P \left[r^{(k)*} \rho^{(k)0} \left(\begin{array}{c} \mathbf{HP}[\mathbf{u}^{(k)'}] \\ - r^{(k)*} \mathbf{D}^{(k)} \nabla P' \\ - r^{(k)'} \mathbf{D}^{(k)} \nabla P' \end{array} \right) \cdot \mathbf{S} \right] \right. \\ & \left. + \frac{(r_P^{(k)*} \rho_P^{(k)0}) - (r_P^{(k)} \rho_P^{(k)})^{Old}}{\delta t} \Omega_P + \right. \\ & \left. \Delta_P \left[\left(r^{(k)*} \rho^{(k)0} U^{(k)*} \right) \right] \right) \\ & = RESG_P \end{aligned} \quad (23)$$

The above equation can be expanded using any simple-like algorithm to yield the new GCBA family of multi-fluid flow algorithms (GCBA-SIMPLE, GCBA-PISO, GCBA-SIMPLEX..)

TEST PROBLEMS

In this section, two two-dimensional two-phase problems are solved. The first problem deals with incompressible turbulent flows while the second problem is concerned with compressible flows.

Turbulent upward bubbly flow in a pipe

The problem considered involves the prediction of radial phase distribution in turbulent upward air-water flow in a pipe. Many experimental and numerical studies addressing this problem have appeared in the literature [15,16,17,18,19]. Most of these studies have indicated that the lateral forces that most strongly affect the void distribution are the turbulent stresses and the lateral lift force. As such, in addition to the usual drag force, the lift force is considered as part of the interfacial force terms in the momentum equations. In the present work, the interfacial drag forces per unit volume are given by:

$$\begin{aligned} (\mathbf{I}_M^{(x,y)})_D^{(c)} &= -(\mathbf{I}_M^{(x,y)})_D^{(d)} \\ &= 0.375 \frac{C_D}{r_p} \rho^{(c)} r^{(d)} r^{(c)} \|V_{slip}\| \left(v_{(x,y)}^{(d)} - v_{(x,y)}^{(c)} \right) \end{aligned} \quad (24)$$

where r_p is the bubble radius. The drag coefficient C_D varies as a function of the bubble Reynolds and Weber numbers defined as:

$$Re_p = 2 \frac{r_p}{v_1^{(c)}} V_{slip}; We = 4 \rho^{(c)} \frac{r_p^2}{\sigma} V_{slip}^2 \quad (25)$$

where σ is the surface tension, which is given a value of 0.072N/m for air-water systems. The following correlations, which take the shape of the bubble into consideration, are utilized [18]:

$$\left\{ \begin{array}{l} C_D = \frac{16}{Re_p} \quad \text{for } Re_p < 0.49 \\ C_D = \frac{20}{Re_p^{0.643}} \quad \text{for } 0.49 < Re_p < 100 \\ C_D = \frac{6.3}{Re_p^{0.385}} \quad \text{for } Re_p \gg 100 \\ C_D = \frac{8}{3} \quad \text{for } Re_p \gg 100 \text{ and } We > 8 \\ C_D = \frac{We}{3} \quad \text{for } Re_p \gg 100 \text{ and } Re_p > 2065.1 / We^{2.6} \end{array} \right. \quad (26)$$

Many investigators have considered the modeling of lift forces [20]. Based on their work, the following expressions are employed for the calculation of the interfacial lift forces per unit volume:

$$(\mathbf{I}_M)_L^{(c)} = -(\mathbf{I}_M)_L^{(d)} = C_1 \rho^{(c)} r^{(d)} (\mathbf{u}^{(d)} - \mathbf{u}^{(c)}) \times (\nabla \times \mathbf{u}^{(c)}) \quad (27)$$

where C_1 is the interfacial lift coefficient calculated from:

$$C_1 = C_{1a} \langle 1 - 2.78 \rangle 0.2, r^{(d)} \quad (28)$$

where $\langle a, b \rangle$ denotes the minimum of a and b and C_{1a} is an empirical constant.

Besides the drag and lift interfacial forces, the effect of bubbles on the turbulent field is very important, since the distribution of bubbles affects the turbulence field in the liquid phase and at the same time the liquid phase's turbulence is influenced by the bubbles. In this work, turbulence is assumed to be a property of the continuous liquid phase (c) and the turbulent kinematic viscosity of the dispersed air phase (d) is assumed to be a function of that of the continuous phase. The turbulent viscosity of the continuous phase is computed by solving a modified transport equations for the turbulent kinetic energy k and its dissipation rate ε that take into account the interaction between the phases. Moreover, as suggested in [18], the flux representing the interaction between the fluctuating velocity and volume fraction is modeled via a gradient diffusion approximation and added as a source term in the continuity $\left(\nabla \cdot (\rho^{(k)} D^{(k)} \nabla r^{(k)}) \right)$ and momentum $\left(\nabla \cdot (\rho^{(k)} D^{(k)} \mathbf{u}^{(k)} \nabla r^{(k)}) \right)$ equations with the diffusion coefficient D given by:

$$D^{(k)} = \frac{v_t^{(k)}}{\sigma_r} \quad (29)$$

The turbulent kinematic eddy viscosity of the dispersed and continuous phases are related through:

$$v_t^{(d)} = \frac{v_t^{(c)}}{\sigma_f} \quad (30)$$

where σ_f is the turbulent Schmidt number for the interaction between the two phases.

To check the validity and correctness of the above-described treatment, the data reported by Seriwaza et al [15] is reproduced. The Reynolds number based on superficial liquid velocity and pipe diameter is 8×10^4 , the inlet superficial gas and liquid velocities are 0.077 and 1.36 m/s, respectively, and the inlet void fraction is 5.36×10^{-2} with no slip between the incoming phases. Moreover, the bubble diameter is taken as 3 mm [18], while the fluid properties are taken as $\rho^{(c)} = 1000 \text{ Kg/m}^3$, $\rho^{(d)} = 1.23 \text{ Kg/m}^3$, and $v_1^{(c)} = 10^{-6} \text{ m}^2/\text{s}$. The problem is solved using the following values for the constants in the model: $C_{1a} = 0.075$, $\sigma_r = 0.5$, $\sigma_f = 0.7$, and $C_b = 0.05$. Predicted radial profiles of the vertical liquid velocity and void fraction presented in Figs. 2(a) concur very well with measurements and compare favorably with numerical profiles reported by Boisson and Malin [18]. The performance of the GCBA in terms of convergence history (Fig. 2(b)) show noticeable similarity between the algorithms this is not surprising since all account for the additional r -coupling. The lower iteration count for GCBA-PISO is due to the two pressure corrections that take place in any one PISO iteration. As for the high iteration count of the PRIME algorithms it is the authors view that this is mainly the result of the explicit treatment of the momentum equations. In the PRIME algorithm

the momentum equations are not solved rather the velocity fields evolves from the successive corrections that occur after solving the pressure correction equation.

Dilute Air-Particle Subsonic Flow over a Flat Plate

This problem has been repeatedly [21,22,23] as a benchmark. It is known that two-phase flow greatly changes the main features of the boundary layer over a flat plate. Typically, three different regions are defined in the two-phase boundary layer (Fig. 3(a)), which can be distinguished by the relative velocity between the two phases: a large-slip region close to the leading edge, a moderate-slip region further down, and a small-slip one far downstream. A more detailed description of the problem can be found in [22]. It is worth noting however that even though variations in gas density are small under the conditions considered, these variations are not neglected and the flow is treated as compressible for the continuous phase and as incompressible for the dispersed phase. The drag is the only interfacial force retained due to its dominance over other interfacial forces and is given by:

$$(\mathbf{I}_M)_D^{(c)} = -(\mathbf{I}_M)_D^{(d)} = \frac{9}{2} \frac{C_D}{r_p^2} r^{(d)} \mu^{(c)} (\mathbf{v}^{(d)} - \mathbf{v}^{(c)}) \quad (31)$$

where the drag coefficient is given by:

$$C_D = \frac{1}{50} \text{Re}_p + \frac{7}{6} \text{Re}_p^{0.15} \quad (32)$$

In the energy equation, heat transfer due to radiation is neglected and only convective heat transfer around an isolated particle is considered. Under such conditions, the interfacial terms in the gas (continuous phase) and particles (dispersed phase) energy equations reduce to **[Error! Bookmark not defined.]**:

$$I_E^{(c)} = Q_{g-p} + \mathbf{F}_{g-p} \cdot \mathbf{u}^{(d)} \quad (33)$$

$$I_E^{(d)} = -Q_{g-p} \quad (34)$$

where:

$$\mathbf{F}_{g-p} = \left(I_M^x \right)_D^{(c)} \mathbf{i} + \left(I_M^y \right)_D^{(c)} \mathbf{j} \quad (35)$$

$$Nu = 2.0 + 0.6 \text{Re}_p^{\frac{1}{2}} \left(\text{Pr}^{(c)} \right)^{\frac{1}{3}} \quad (36)$$

$$Q_{g-p} = \frac{3}{2} \frac{r^{(d)} \lambda^{(c)} Nu}{r_p^2} (T^{(d)} - T^{(c)}) \quad (37)$$

In the above equations, Nu is the Nusselt number, $\text{Pr}^{(c)}$ the gas Prandtl number, $\lambda^{(c)}$ the gas thermal conductivity, T the temperature, and other parameters are as defined earlier.

The particle diameter is chosen to be 10 μm , the particle Reynolds number is assumed to be equal to 10, and the material density is 1766 kg/m^3 . The Prandtl number is equal to 0.75. The south boundary (wall) is treated as a no-slip wall boundary for the gas phase: both components of the gas velocity are set to zero, while the particle phase encounters slip wall conditions. The normal fluxes are set

to zero. The gas and the particles enter the computational domain under thermal and dynamical equilibrium conditions. A mass load ratio of 1 between the particles phase and the gas phase is used. Results are displayed using the following dimensionless variables in order to bring all quantities to the same order of magnitudes:

$$\begin{aligned} x^* &= \frac{x}{\lambda_e}, y^* = \frac{y}{\lambda_e} \sqrt{\text{Re}}, \\ u^* &= \frac{u}{u_\infty}, v^* = \frac{v}{u_\infty} \sqrt{\text{Re}} \quad \text{Re} = \frac{\rho u \lambda_e}{\mu} \end{aligned} \quad (38)$$

Figure 3(b) shows the results for the steady flow obtained on a rectangular domain with a mesh of density 104x48 C.V. stretched in the y-direction. The figure provides the development of gas and particles velocity profiles within the three regions mentioned earlier. In the near leading edge area ($x^*=0.1$), the gas velocity is adjusted at the wall to obtain the no-slip condition as for the case of a pure gas boundary layer. The particles have no time to adjust to the local gas motion and there is a large velocity slip between the phases. In the transition region ($x^*=1$), significant changes in the flow properties take place. The interaction between the phases cause the particles to slow down while gas accelerate as apparent in the plots. In the far downstream region ($x^*=5$), the particles have enough time to adjust to the state of the gas motion. The slip is very small and the solution tends to equilibrium. These results are in excellent agreement with numerical solutions reported by Thevand et al. [23] plotted in Fig. (6(b)), which gives credibility to the proposed methodology. The convergence histories of the various algorithms are presented in Fig. 7. Consistently, PISO and PRIME require the lowest and highest number of iterations, while the performance of all other GCBA is close.

CONCLUDING REMARKS

In this paper a new class of multi-fluid algorithms by was presented and seven GCBA-based segregated solvers were tested in two problems involving incompressible and compressible fluids. The convergence histories of all the GCBA-based solvers were found to be very similar in both problems. This is, in the authors' view, an effect of implicitly resolving the geometric conservation law as part of the velocity-pressure (and density) coupling.

REFERENCES

- [1] Darwish, M., Moukalled, F., and Sekar, B., "A Unified Formulation of the Segregated Mass Conservation Based Algorithms for Multi-Fluid Flow at All Speeds," 36th AIAA/ASME/SAE/ ASEE Joint Propulsion Conference, Huntsville, Alabama, 16-19 July 2000.
- [2] Patankar, S.V., Numerical Heat Transfer and Fluid Flow, Hemisphere, N.Y., 1981.
- [3] Issa, R.I., "Solution of the Implicit Discretized Fluid Flow Equations by

Operator Splitting," Mechanical Engineering Report, FS/82/15, Imperial College, London, 1982.

- [4] Van Doormaal, J. P. and Raithby, G. D. "An Evaluation of the Segregated Approach for Predicting Incompressible Fluid Flows," ASME Paper 85-HT-9, Presented at the National Heat Transfer Conference, Denver, Colorado, August 4-7, 1985.
- [5] Moukalled, F. and Darwish M.S., "A Unified Formulation of the Segregated Class of Algorithms for Fluid Flow at All Speeds", Numerical Heat Transfer, (in press).
- [6] Spalding, D.B., "The Calculation of Free-Convection Phenomena in Gas-Liquid Mixtures" Report HTS/76/11 Mech. Eng. Imperial College, London, 1976.
- [7] Spalding, D.B., "Numerical Computation of Multi-Phase Fluid Flow and Heat Transfer", in Recent Advances in Numerical Methods in Fluids eds Taylor C., Morgan K., pp. 139-167, vol. 1, 1980.
- [8] Spalding, D.B., "A General Purpose Computer Program for Multi-Dimensional, One and Two Phase Flow", Report HTS/81/1 Mech. Eng. Imperial College, London, 1981.
- [9] Harlow, F.M., Amsden, A.A., "Numerical calculations of Multiphase Flow", Journal of Computational Physics, vol 17, pp. 19-52, 1975.
- [10] Stewart, H.B., "Stability of Two-Phase Flow Calculation Using Two-Fluid Models," Journal of Computational Physics, vol 33, pp. 259-270, 1979.
- [11] Rivard, W.W. and Torrey, M.D., "KFIX: A Program for Transient Two Dimensional Two Fluid Flow", Report LA-NUREG-6623, 1978
- [12] Mahaffy, J.H., "A Stability Enhancing Two-Step Method for One Dimensional Two-Phase Flow", Report NUREG/CR-0971, 1979.
- [13] Stewart, H.B., "Fractional Step Methods for Thermohydraulic Calculation," Journal of Computational Physics, vol 40, pp. 77-80, 1981.
- [14] Stewart, H.B. and Wendroff, B., "Two-Phase Flow: Models and Methods", Journal of Computational Physics, vol 56, pp. 363-409, 1984.
- [15] Serizawa, A., Kataoka, I., and Michiyoshi, I., "Phase Distribution in Bubbly Flow," Data set No. 24, Proceedings of the Second International Workshop on Two-Phase Flow Fundamentals, Rensselaer Polytechnic Institute, Troy, NY, 1986.
- [16] Wang, S.k., Lee, S-j, Jones, Jr., O.C., and Lahey, Jr., R.T., "3-D Turbulence structure and Phase Distribution Measurements in Bubbly Two-Phase Flows," International Journal of Multiphase Flow, vol. 13, No. 3, 1987.
- [17] Lopez de Bertodano, M., Lahey, Jr., R.T., and Jones, O.C., "Development of a k-Model for Bubbly Two-Phase Flow," Journal of Fluids Engineering, vo. 116, pp. 128-134, 1994.
- [18] Boisson, N. and Malin, M.R., "Numerical Prediction of Two-Phase Flow in Bubble Columns," International Journal for Numerical Methods in Fluids, vol. 23, pp. 1289-1310, 1996.
- [19] Nakoryakov, V.E., Kashinsky, O.N., Randin, V.V., and Timkin, L.S., "Gas-Liquid Bubbly Flow in Vertical Pipes," Journal of Fluids Engineering, vo. 118, pp. 377-382, 1996.
- [20] Lahey, R.T., Lopez de Bertodano, M., and Jones, O.C., "Phase Distribution in Complex Geometry Ducts," Nuclear Engineering Design, vol. 141, p. 177, 1993.
- [21] Osipov, A.N., "Structure of the Laminar Boundary Layer of a Disperse Medium on a Flat Plate," Fluid Dyn., vol. 15, pp. 512-517, 1980.
- [22] Wang, B.Y., and Glass, I.I., "Compressible Laminar Boundary Layer Flows of a Dusty Gas Over a Semi-Infinite Flat Plate," Journal of Fluid Mechanics, vol. 186, pp. 223-241, 1988
- [23] Thevand, N., Daniel, E., and Loraud, J.C., "On high-Resolution Schemes for Solving Unsteady Compressible Two-Phase Dilute Viscous Flows," International Journal of Numerical Methods in Fluids, vol. 31, pp. 681-702, 1999.

FIGURES

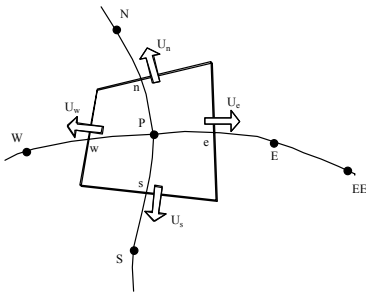
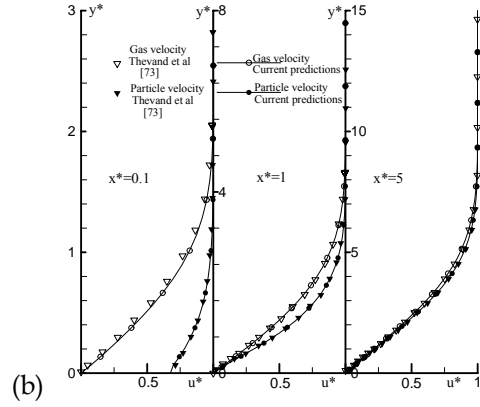
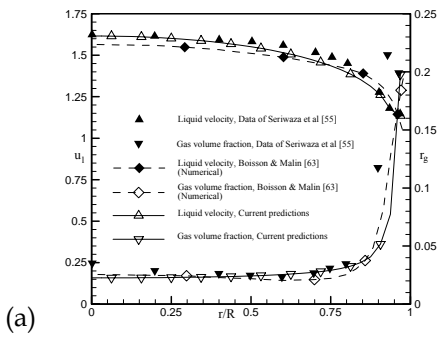


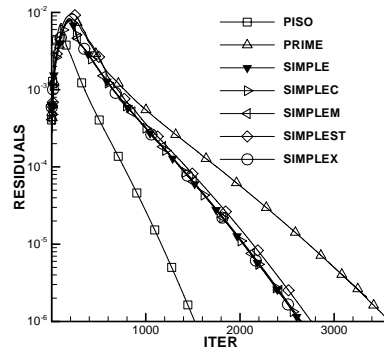
Figure 1: Control Volume



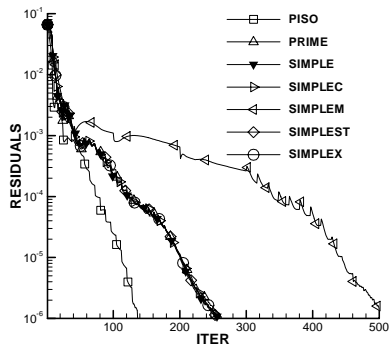
(b)



(a)



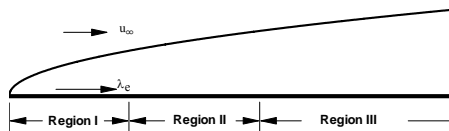
(c)



(b)

Figure3: (a) The three different regions within the boundary layer of dusty flow over a flat plate, (b) Comparison of fully developed gas and particle velocity profiles inside the boundary layer at different axial locations for dilute two-phase flow over a flat plate

Figure 2: (a) Comparison of fully developed liquid velocity and void fraction profiles for turbulent bubbly upward bubbly flow in a pipe against Seriwaza et al. data, (b) Convergence history of the various multi-phase algorithms



(a)